Hydrodynamical analysis of symmetric nucleus-nucleus collisions near 200*A* GeV

U. Ornik,[1,*] M. Plümer,[2,†] B.R. Schlei,[3,‡] D. Strottman,[3,§] and R.M. Weiner[2,‖]
[1]*SoulTek Internet Services, Software Center 5, Marburg, Germany*
[2]*Physics Department, University of Marburg, Marburg, Germany*
[3]*Theoretical Division, Los Alamos National Laboratory, Los Alamos, New Mexico 87545*
(Received 12 April 1996)

We present a coherent theoretical study of ultrarelativistic heavy-ion data obtained at the CERN/SPS by the NA35/NA49 Collaborations using (3+1)-dimensional relativistic hydrodynamics. We find excellent agreement with the rapidity spectra of negative hadrons and protons and with the correlation measurements in two experiments: S+S at 200*A* GeV and Pb+Pb at 160*A* GeV (preliminary results). Within our model this implies that for Pb+Pb (S+S) a quark-gluon plasma of initial volume 174 fm^3 (24 fm^3) with a lifetime 3.4 fm/c (1.5 fm/c) was formed. It is found that the Bose-Einstein correlation measurements do not determine the maximal effective radii of the hadron sources because of the large contributions from resonance decay at small momenta. Also within this study we present an NA49 acceptance-corrected two-pion Bose-Einstein correlation function in the invariant variable $Q_{\rm inv}$. [S0556-2813(96)03209-8]

PACS number(s): 25.75.−q, 12.38.Mh, 24.10.Jv, 24.10.Nz

I. INTRODUCTION

In the last decade many experiments have been performed in the attempt to find evidence for the existence of a quark-gluon plasma (QGP). Ever higher energies and/or masses have been involved in order to increase the lifetime of the system either by increasing the initial energy density or the size of the system. The probability of preparing a strongly interacting system that shows thermodynamical behavior and therefore is treatable by well-known thermodynamical or fluid dynamical methods increases with the size of the system. In this paper we describe a comprehensive hydrodynamical study of data taken at the CERN/SPS by the NA35 and the NA49 Collaborations. Our investigation takes into account all available data spectra and correlation functions for different particle species. We present results of the analysis [1] of Pb+Pb at 160*A* GeV using relativistic fluid dynamics and assuming an equation of state containing a phase transition. These results are discussed by comparison to our previous findings for S+S at 200*A* GeV which were obtained by applying the same computer code HYLANDER [2].

Many hydrodynamical models [3–5] are available which describe the dynamics of relativistic heavy-ion collisions. HYLANDER belongs to the class of models which apply (3+1)-dimensional relativistic one-fluid dynamics. It provides fully three-dimensional solutions of the hydrodynamical relativistic Euler equations [6]. HYLANDER has been successfully applied at SPS energies to the reaction Au+O and especially to S+S, a reaction to which we refer several times in this paper. Here HYLANDER was used to reproduce [7] simultaneously mesonic and baryonic rapidity and transverse momentum spectra of the S+S reaction at 200*A* GeV. Corresponding measurements had been performed by the NA35 Collaboration [8]. Based on the successful description of the measured single inclusive spectra, predictions were made for Bose-Einstein correlation (BEC) functions [9,10]. Those predictions agree quantitatively with the measurements [11,12] (cf. also Fig. 9). The model also reproduces the photon data for S+Au collisions at SPS energies [13] and gives a simple explanation for the ''soft-$p_\perp$ puzzle'' [14] and the complex behavior of the radii extracted from pion and kaon correlations and explains the difference in the extracted radii for pions and kaons in terms of a cloud of pions due to the decay of resonances which surrounds the fireball (pion halo) [9,15].

In the present paper we exhibit the space-time geometries of the real hadron sources, i.e., the freeze-out hypersurfaces. Results for S+S at 200*A* GeV and Pb+Pb at 160*A* GeV are directly compared. For the first time we show our results of effective radii compared to the BEC data of the NA35 Collaboration. Furthermore, we present a calculation of the detector-acceptance-corrected two-pion correlation function $\widetilde{C}_2(Q_{\rm inv})$ in the invariant variable $Q_{\rm inv}$. In doing so we would like to bring the readers attention also to Refs. [16,17] where all the features of these specific types of two-particle BEC functions were extensively discussed. The following discussion is a self-consistent description of two different heavy-ion experiments. Here we reproduce simultaneously single inclusive spectra of negative hadrons and protons and Bose-Einstein correlations of identical pions using only one and the same equation of state. The contents of this paper represents a summary of many contributions [1,2,7,9,10,18] in an effort to give a description of heavy-ion data taken at the CERN/SPS in terms of (3+1)-dimensional relativistic hydrodynamics.

II. MODELING THE HYDRODYNAMICAL SOLUTIONS

HYLANDER can use initial conditions ranging between the extremes defined by the Landau [19] and the Bjorken [20] initial conditions. One has to specify an equation of state and a set of parameters which describe the initial conditions. In

*Electronic address: ornik@warp.soultek.de
†Electronic address: pluemer@Mailer.Uni-Marburg.DE
‡Eelectronic address: schlei@t2.LANL.gov
§Electronic address: dds@LANL.gov
‖Electronic address: weiner@Mailer.Uni-Marburg.DE

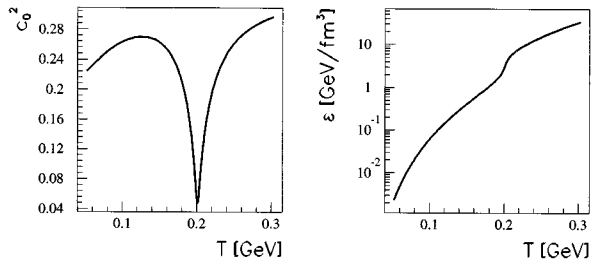

FIG. 1. Equation of state with a phase transition to a quark-gluon plasma. Plotted are the speed of sound c_0^2 and the energy density ϵ as a function of temperature T [23]. The curves are a result of a fit [22] to lattice QCD calculations [21].

view of our former results for S+S at 200*A* GeV, the same equation of state (EOS) is used for the treatment of Pb+Pb at 160*A* GeV. It exhibits a phase transition to a quark-gluon plasma at a critical temperature $T_c = 200$ MeV (cf. Refs. [21–23]). This EOS, which has no dependence on the baryon density, is plotted in Fig. 1. In the following we sketch the basic features of the model which was introduced in Ref. [7]. Our model uses the five parameters K_L, Δ, y_Δ, y_m, and σ, which are explained below.

A reaction of two baryonic fluids leads to a deceleration of the projectile and target baryonic currents and thus to the spread of their width in momentum space. For the initial baryon density distribution in rapidity we write

$$\frac{db}{dy} = C_y[e^{-(y-y_m)/2\sigma^2} + e^{-(y+y_m)/2\sigma^2}], \tag{1}$$

where $\pm y_m$ give the positions in rapidity of the two maxima and σ gives the width of the baryonic density distribution after the collision, respectively. C_y is a normalization constant, the value of which can be determined from the requirement that, when Eq. (1) is integrated over the whole accessible rapidity interval, it is equal to the total baryon number of the system. A spatial baryon distribution (cf. Fig. 2) is then easily derived by evaluating

$$B_0(z) = \frac{1}{\pi R^2}\frac{db}{dy}\frac{dy}{dz}, \tag{2}$$

where R is the mean radius of the initially radially smeared out cylindrical fireball (cf. Ref. [10]). In our model we impose an initial rapidity field $y(z)$ on the fluid. Its modulus is presumed to be a function only of the longitudinal coordinate z with its shape constrained by two boundary values: The rapidity should vanish at $z=0$ and asymptotically reach its maximum value $y_{\text{c.m.}}$ at $z=\pm t_a$ ($y_{\text{c.m.}}$ being the center-of-mass rapidity and t_a the time it takes for two nuclei at the speed of light to penetrate each other, respectively). We parametrize the function $y(z)$ by the slope parameter a_y as

$$y(z) = y_{\text{c.m.}}\tanh[a_y|z|]. \tag{3}$$

Rather than using a_y as a free parameter in our model, we use the two parameters Δ and y_Δ determining the slope parameter a_y in Eq. (3) through

$$y(z=\pm\Delta/2) = y_\Delta. \tag{4}$$

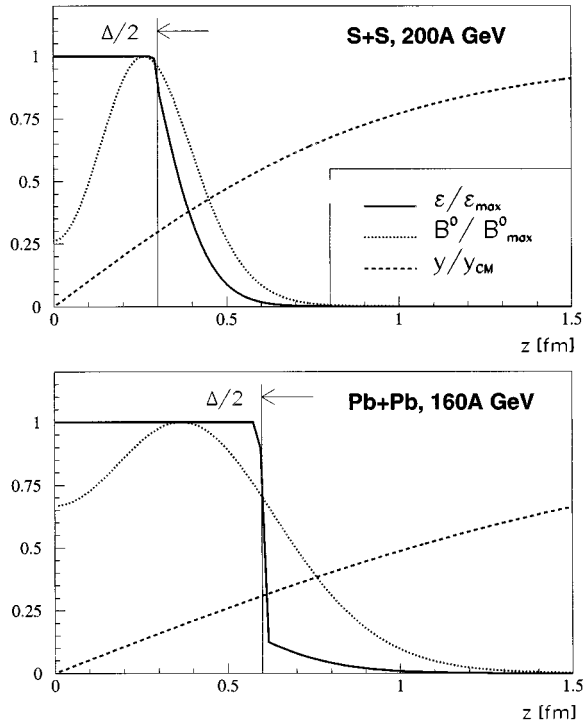

FIG. 2. Initial distributions of energy and baryon density, as well as the rapidity, normalized to their maximum values (cf. Table I) and plotted against the longitudinal coordinate z.

In Eq. (4) the quantity Δ is the spatial longitudinal extension of the initial fireball (in Ref. [7] called the ''Landau volume'') and y_Δ is the absolute value of rapidity at $z=\pm\Delta/2$.

The kinetic energy of the two incoming baryonic fluids is converted into internal excitation (thermal energy) of a third fluid which is created in the central region. The relative fraction K_L of the thermal energy inside the initial fireball volume is another free parameter which fixes the initial state of the formed fireball.

In Table I we show the choice of the five parameters which leads to the reproduction of the experimental S+S data taken by the NA35 Collaboration. Additionally, it was there assumed that due to experimental uncertainty for the centrality of the collision, only 85% of the total available energy and the total baryon number have been observed. In Fig. 2 the initial longitudinal distributions of energy density, as well as the rapidity, normalized to their maximum values are plotted against the longitudinal coordinate z (since we deal with a symmetric system, only the distributions for $z \geqslant 0$ are shown). Because of the constraints of energy conservation, the choice of the initial parameters Δ, y_Δ, and σ leads to a limited two-parameter space for the variables K_L and y_m, respectively. The limited two-parameter space is shown for S+S in Fig. 3. The crossed lines indicate the choice of the parameter pair for the reproduction of the heavy-ion data.

For Pb+Pb at 160*A* GeV we reduce our five-parameter space to a two-parameter space based on the results we obtained for S+S at 200*A* GeV. We assume that the parameter for the longitudinal extension of the central fireball scales with $2R/\gamma$ compared to the parameter for S+S at 200*A* GeV

TABLE I. Properties of initial fireball extracted from a hydrodynamical analysis of the S+S NA35 data [8] and the Pb+Pb NA49 data [25,26].

	S+S	Pb+Pb
Fit parameters		
Rel. fraction K_L of thermal energy in the central fireball	0.43	0.65
Longitudinal extension Δ of central fireball	0.6 fm	1.2 fm
Rapidity y_Δ at edge of central fireball	0.9	0.9
Rapidity y_m at maximum of initial baryon distribution	0.82	0.60
Width σ of initial baryon y distribution	0.4	0.4
Output		
Center of mass rapidity $y_{\text{c.m.}}$	3.03	2.92
Max. initial energy density, $\epsilon_{\max}$	13.0 GeV/fm^3	20.4 GeV/fm^3
Max. initial baryon density, $B^0_{\max}$	2.66 fm^{-3}	3.20 fm^{-3}
Rel. fraction of baryons in central fireball	0.49	0.73
Max. lifetime	6.9 fm/c	13.5 fm/c
Initial volume of QGP	24 fm^3	174 fm^3
Lifetime of QGP	1.5 fm/c	3.4 fm/c
Max. halo size in ''longitudinal'' direction	2.5 fm	5.6 fm
Max. halo size in ''side'' direction	1.0 fm	2.4 fm
Max. halo size in ''out'' direction	1.3 fm	2.6 fm

[1]; γ is the Lorentz contraction factor. By coincidence there is a factor of 2 increase in the longitudinal extension Δ going from the reaction S+S at 200A GeV to Pb+Pb at 160A GeV. Also the time t_a it takes for two nuclei at the speed of light to penetrate each other is increased by a factor of 2. For S+S the initial longitudinal velocity field $v_\parallel(z)=\tanh[y(z)]$ increases as a function of z within the initial fireball almost linearly as in the Bjorken initial condition scenario [there $v_{\text{Bjorken}}(z)=z/\tau$; τ is a time scale which can be identified with t_a]. Since Δ and t_a each scale with a factor of 2, by using the Bjorken scaling argument for the initial longitudinal velocity field, the increase of the initial longitudinal rapidity field with the coordinate z is reduced almost by a factor of 0.5 for Pb+Pb compared to S+S, which results in the same choice for the initial parameter $y_\Delta=y(z=\Delta/2)$ for both reactions.

We have checked that the variation of the width σ of the initial baryon density distribution to a large extent does not affect the calculation of rapidity spectra. Therefore, the value of σ remained unchanged. The values of Δ, y_Δ, and σ are given in Table I. Thus we are left with *only two* parameters: the relative fraction of the thermal energy K_L in the central fireball and the rapidity y_m at the maximum of the initial baryon distribution. Figure 3 shows the corresponding limited two-parameter space for Pb+Pb at 160A GeV due to energy conservation. The crossed lines indicate our choice

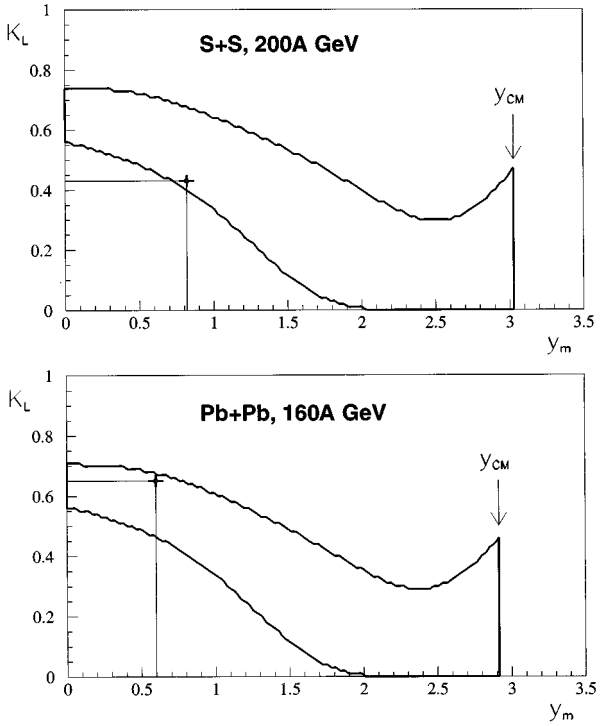

FIG. 3. Boundaries in the two-parameter planes for the relative fraction K_L of thermal energy in the central fireball and the rapidity y_m at the maximum of the initial baryon distribution, respectively. The crossed lines indicate our particular choices for the calculations.

for the two parameters which are determined by fitting the rapidity spectrum of negative hadrons of the preliminary NA49 data. All other spectra and correlation functions, which will be discussed below, are predictions of the model. Because of the preliminary state of the NA49 data we decided to perform a calculation for the choice of an impact parameter $b_{\text{imp}}=0$. Figure 2 shows the initial longitudinal distributions of energy density as well as the rapidity, normalized to their maximum values (cf. Table I) as a function of the longitudinal coordinate z.

III. DISCUSSION OF THE HYDRODYNAMICAL SOLUTIONS

Once the initial conditions and the equation of state are specified, one obtains an unambiguous solution from the hydrodynamical relativistic Euler equations. In our calculations we assume that hadronization occurs for all particle species at the same fixed freeze-out energy density ϵ_f. Since our equation of state is not dependent on the baryon density, the freeze-out energy density easily translates into a fixed freeze-out temperature T_f. Our choice for the freeze-out temperature is $T_f=139$ MeV.

The choice of a fixed freeze-out temperature T_f determines the final space-time geometry of the hydrodynamically expanding fireball. In Fig. 4 we have plotted the freeze-out regions at different times for directly produced hadrons in the z-r plane for S+S at 200A GeV and for Pb+Pb at 160A GeV, respectively. Each line represents the freeze-out hypersurface at fixed times t. One can see very easily that the solutions we obtained from our numerical analysis represent

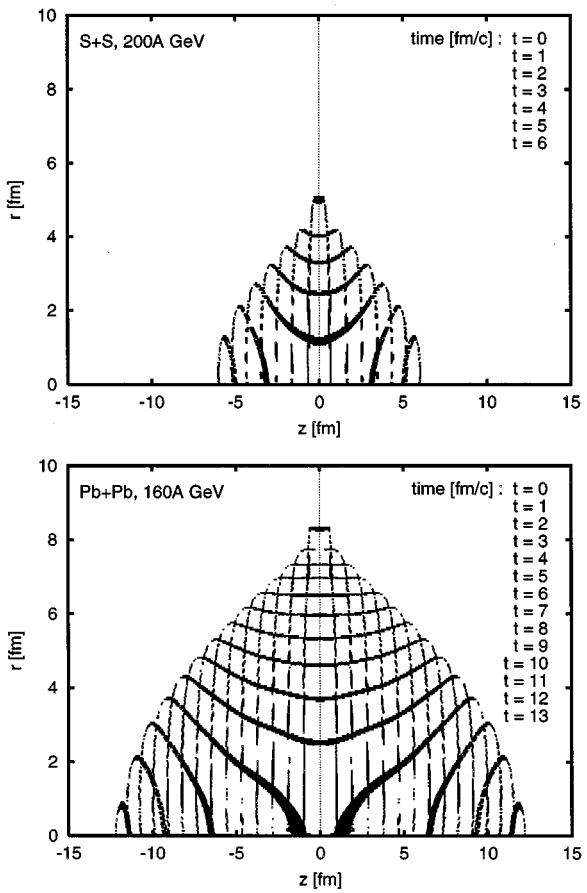

FIG. 4. Time contour plots of the freeze-out hypersurfaces in the z-r plane. Each line represents the freeze-out hypersurface at a fixed time t.

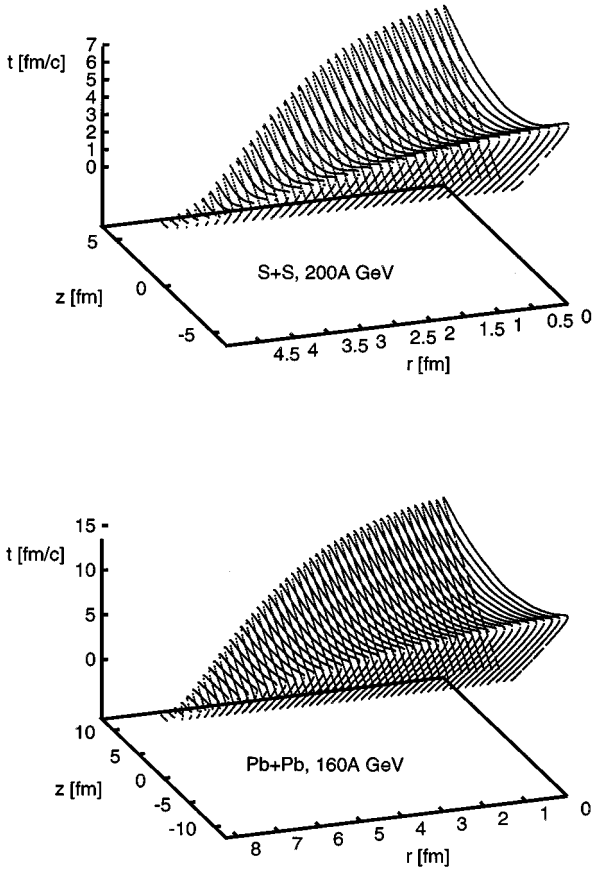

FIG. 5. Three-dimensional view of the freeze-out hypersurfaces.

an evolution of initially disk-shaped fireballs which emit hadrons from the very beginning of their formation. While the relativistic fluids expand in longitudinal and in transverse directions, the longitudinal positions of the freeze-out points increase their distance relative to the center. Because of the effect of transverse inwardly moving rarefaction waves, the transverse freeze-out positions move towards the center of the fireball (cf. also Ref. [18]). In the late stage of the hydrodynamical expansion the hadron-emitting fireballs separate into two parts while cooling down until they cease to emit.

In Fig. 5 we give the full three-dimensional views of the freeze-out hypersurfaces of directly emitted hadrons for S+S at 200A GeV as well as for Pb+Pb at 160A GeV. The freeze-out space-time geometries show a similar behavior for both heavy-ion reactions although the longitudinal and transverse sizes of the systems differ approximately by a factor of 2.

Above we have argued that the initial parameters Δ and y_Δ have geometrical scaling features, while σ remains unchanged. The only parameters which were chosen freely (except for the constraint of energy conservation) are K_L and y_m (cf. Fig. 3). Consistent with expectation the degree of stopping and thermalization is higher in Pb+Pb and the amount of thermal energy (represented by the parameter K_L) in the central fireball increases from 43% (S+S) to 65% (Pb+Pb). The location of the maximum density of the two baryon currents, y_m, in rapidity space is significantly shifted into the central rapidity region. The baryons for Pb+Pb are almost stopped. The resulting high baryonic density in the Pb+Pb case of 2.14 fm^{-3} in the center is 3 times higher than in S+S. In the Pb+Pb case 73% of the baryons are initially located in the central region compared to only 49% in the S+S case (cf. Fig. 2).

In Fig. 6 we give for both reactions three-dimensional views of corresponding transverse velocities at freeze-out. The two systems each show a maximum value for the transverse velocities: For S+S at 200A GeV we obtain a maximum transverse velocity $u_\perp^{\max}(S)=0.43$, whereas for Pb+Pb at 160A GeV we get $u_\perp^{\max}(\mathrm{Pb})=0.61$. But the slope of the transverse increase of the transverse velocity $u_\perp$ is smaller for the Pb+Pb system compared to the S+S system. The reason for this different behavior has its origin in the different choice of the initial parameters: Because of a higher initial thermal energy density, the internal pressure of the Pb+Pb system is increased compared to S+S, resulting in a relatively faster longitudinal and transverse expansion of the relativistic fluid. The rarefaction waves in Pb+Pb also move inwardly faster and inhibit the creation of an adequate large transverse velocity field at freeze-out, yielding a smaller transverse slope for $u_\perp$ compared to S+S.

From our calculations we find that for Pb+Pb a quark-gluon-plasma with an initial volume of 174 fm^3 was formed while for S+S there is a QGP with an initial volume of 24 fm^3. The maximum lifetime of the fireball is increased from 6.9 fm/c (S+S) up to 14.5 fm/c for Pb+Pb. We observe approximately the same behavior for the lifetimes of the QGP. Whereas in S+S the lifetime of the QGP was short

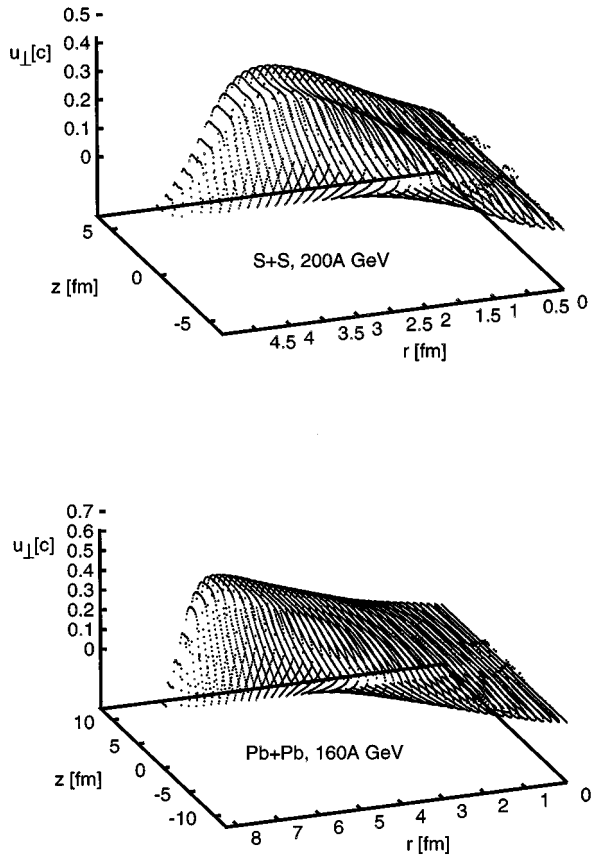

FIG. 6. Three-dimensional view of the transverse velocity fields at freeze-out.

(1.5 fm/c), in the Pb+Pb case a QGP persists for 3.4 fm/c. The latent heat of the phase transition is of the order of 1 GeV/fm^3 (cf. Fig. 1). Taking into account that the initial volume of the Pb+Pb system is approximately eight times larger than in the S+S case, we note that the lifetime increases slower than does the volume. This effect is due to the cooling by transverse rarefaction waves which are only sensitive to the difference in the transverse radius which differs approximately by a factor of two from S+S to Pb+Pb.

IV. SINGLE INCLUSIVE SPECTRA AND BOSE-EINSTEIN CORRELATIONS

In the following we discuss some of the results for the single and double inclusive spectra of mesons and baryons. All calculations are based on thermal as well as on chemical equilibrium. In both types of spectra we include the effect of resonance decays. The influence of partial coherence [10] will not be considered here.

The calculation of single-particle inclusive spectra with HYLANDER was extensively discussed in Ref. [7]. In particular, the momentum distributions are calculated in terms of the generalized Cooper-Frye formula (see Ref. [24]), where explicitly a baryon and a strangeness chemical potential have to be taken into account. These potentials have to be introduced, because the assumption of chemical equilibrium requires zero strangeness and (in general) nonzero baryon density at each freeze-out point. In detail one has to solve the following system of equations for each surface point of given

TABLE II. Chemical compositions of mesons, baryons, and antibaryons at freeze-out for S+S at 200A GeV and Pb+Pb at 160A GeV. Listed are their relative fractions.

Particle species	Mass [GeV/c^2]	S+S	Pb+Pb
π (stable)	0.139	51.094 %	49.201 %
ω	0.783	2.452 %	2.304 %
η'	0.958	0.297 %	0.279 %
η	0.549	2.941 %	2.765 %
ρ	0.770	7.429 %	6.980 %
K^+ (stable)	0.494	7.689 %	7.763 %
K^0	0.498	2.573 %	2.582 %
Λ	1.116	1.174 %	1.356 %
Σ	1.193	2.232 %	2.578 %
Δ	1.232	4.115 %	5.014 %
N (stable)	0.939	9.009 %	10.960 %
$K^\star$	0.893	0.952 %	0.954 %
$\Sigma^\star$	1.386	0.613 %	0.707 %
Ξ	1.320	0.497 %	0.541 %
K^- (stable)	0.494	4.400 %	3.881 %
anti-K^0	0.498	1.472 %	1.289 %
anti-Λ	1.116	0.049 %	0.036 %
anti-Σ	1.193	0.092 %	0.068 %
anti-Δ	1.232	0.098 %	0.066 %
anti-N (stable)	0.939	0.215 %	0.147 %
anti-$K^\star$	0.893	0.546 %	0.479 %
anti-$\Sigma^\star$	1.386	0.025 %	0.019 %
anti-Ξ	1.320	0.036 %	0.028 %

baryon density b in its rest frame:

$$\sum_i b_i n_i(\mu_B,\mu_S)=b, \quad \sum_i s_i n_i(\mu_B,\mu_S)=s=0. \quad (5)$$

The index i enumerates all resonances and their antiparticles. In Eq. (5), b_i, s_i, and $n_i(\mu_B,\mu_S)$ denote the corresponding baryon number, strangeness, and number density of the ith resonance, respectively. For S+S at 200A GeV we find average values for the baryonic chemical potential $\langle\mu_B\rangle=284$ MeV and for the strangeness chemical potential $\langle\mu_S\rangle=44$ MeV using $T_f=139$ MeV for the freeze-out temperature. For Pb+Pb at 160A GeV we find average values $\langle\mu_B\rangle=363$ MeV and $\langle\mu_S\rangle=69$ MeV using the same freeze-out temperature. As a result, we obtain the chemical compositions of hadrons at freeze-out listed in Table II (cf. also Ref. [7]). We stress that due to our choice of the freeze-out temperature of $T_f=139$ MeV, there are large resonance contributions (40%–50%) to the pionic spectra.

Figures 7 and 8 show our model calculations for negative hadrons h^- and protons p for S+S at 200A GeV and Pb+Pb at 160A GeV, respectively. The spectra of negative hadrons h^- are made up by contributions from negatively charged pions and kaons (directly emitted ones plus those originating from the decay of resonances). The K^- spectra consist mainly of directly emitted kaons; less than 10% come from the $K^\star$ resonance. In the case of the NA35 data we obtained our fit parameters (cf. Table I) from a simultaneous fit to the rapidity and transverse momentum spectra for the negative hadrons h^- and the protons p (for the S+S reaction the

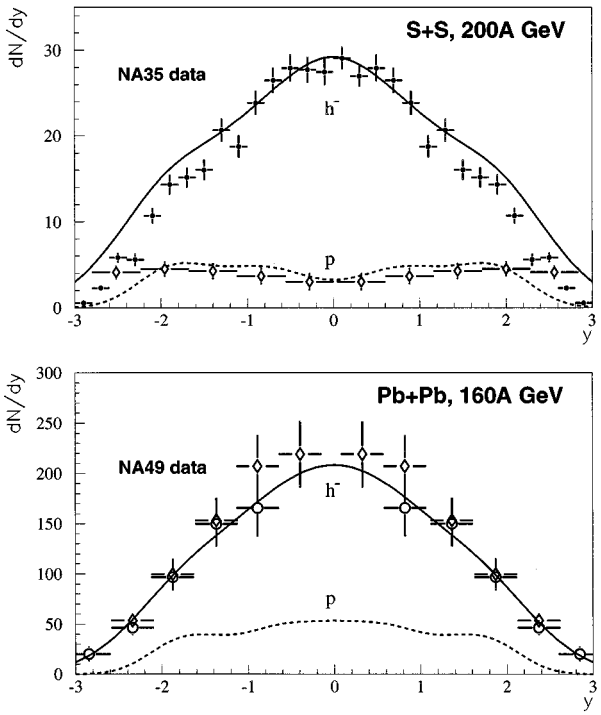

FIG. 7. Rapidity spectra for negative hadrons (h^-) and protons (p). The data points of the NA35 data are taken from [8]. The data points of the preliminary results of the NA49 Collaboration for negative hadrons from central Pb+Pb collisions at 160A GeV are shown with two different markers. Circles (diamonds) stand for the measurements from the VTP2 (MTPC) (cf. Refs. [25,26]).

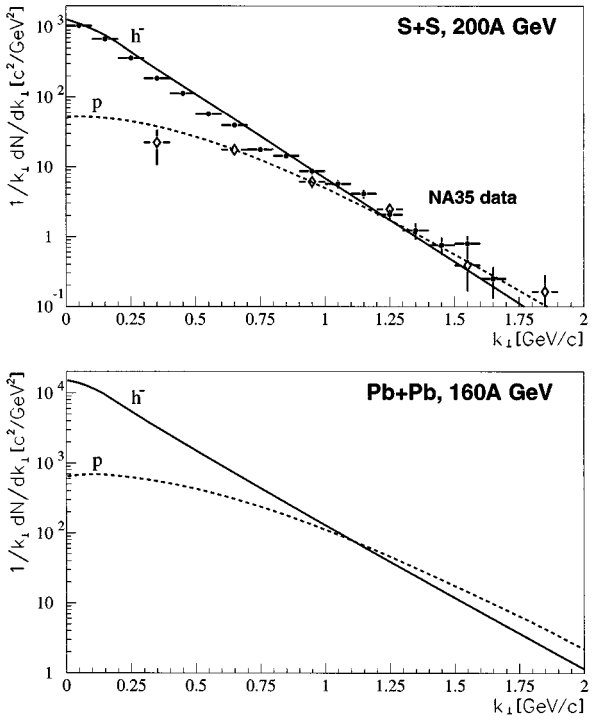

FIG. 8. Transverse momentum spectra of negative hadrons (h^-) and protons (p). The data points of the NA35 data are taken from [8]. For Pb+Pb at 160A GeV the integrations with respect to rapidity y have been performed over the interval $|y| \leq 3.0$.

proton spectra do not include contributions from Λ decays [7] while they do in the treatment of the reaction Pb+Pb). By fitting the h^- rapidity spectrum of the NA49 data we also made sure that the calculated proton rapidity spectrum reproduces simultaneously values observed in the NA44 experiment [27]. In the case of the Pb+Pb data the transverse momentum spectra were not involved in finding a parameter set for the fit of experimental data and are therefore predictions. We mention that unlike in the presentation of Ref. [1], we now account in our calculations for the asymmetric n/p ratio, which is 125/82 for Pb nuclei and which results in an approximately 20% smaller proton spectrum than already shown in [1]. The feature of higher stopping in the Pb+Pb collision scenario is nicely reflected in the rapidity spectra of the protons. While the rapidity spectrum for protons in the S+S case has a minimum at $y=0$, for Pb+Pb, the rapidity spectrum of protons shows a maximum.

The calculation of Bose-Einstein correlations (BEC's) was performed using the formalism outlined in Refs. [9,10,18] including the decay of resonances. The hadron source is assumed to be fully chaotic. Here we present results for pion BEC's only. Kaon correlations have been discussed in Refs. [1,9,10]. In order to extract effective hadron source radii, we fit our results to the Gaussian form[1] which has been widely used by experimentalists for the presentation of their BEC data (for the choice of the variables; cf., e.g., Ref. [10]):

$$C_2(\vec{k}_1,\vec{k}_2) = 1 + \lambda \exp[-\tfrac{1}{2}(q_\parallel^2 R_\parallel^2 + q_{\rm side}^2 R_{\rm side}^2 + q_{\rm out}^2 R_{\rm out}^2)]. \tag{6}$$

It should be emphasized that in the present model λ does *not* represent the effect of coherence, but the momentum-dependent effective reduction of the intercept due to the contributions from the decay of long-lived resonances (cf. [1], [9]).

Figures 9 and 10 show our calculations for the effective radii $R_\parallel$, $R_{\rm side}$, and $R_{\rm out}$ as functions of rapidity y_K and transverse momentum $K_\perp$ of the pion pair compared to the corresponding NA35 and preliminary NA49 data [11,12], respectively. In order to make possible a comparison of the calculated effective radii with the experimentally obtained ones, we have to account for detector acceptances. In the case of S+S at 200A GeV the effective radii as a function of y_K have been calculated at $K_\perp = 200$ MeV, while the effective radii as a function of $K_\perp$ have been calculated at $y_K = 4.0 - y_{\rm c.m.} \approx 1.0$. In the case of Pb+Pb at 160A GeV the effective radii as a function of $K_\perp$ were calculated at $y_K = 4.5 - y_{\rm c.m.} \approx 1.6$. The effective longitudinal radii $R_\parallel$ as a function of $K_\perp$ are evaluated in the longitudinal comoving system (LCMS). All our calculations, which in the case of S+S have been true predictions, agree surprisingly well with the data. In Refs. [1,9,10] we have shown also the effective radii for both types of heavy-ion collisions for $y_K = 0.0$ and $K_\perp = 0.0$. There the effective radii take even larger values compared to the ones we show here when comparing them to the data, because the contributions from resonance decays to

[1]If one performs a fit to a BEC function in more than one dimension, Eq. (6) does not represent the most general expression, because of the existence of an ''out-longitudinal'' cross term [28].

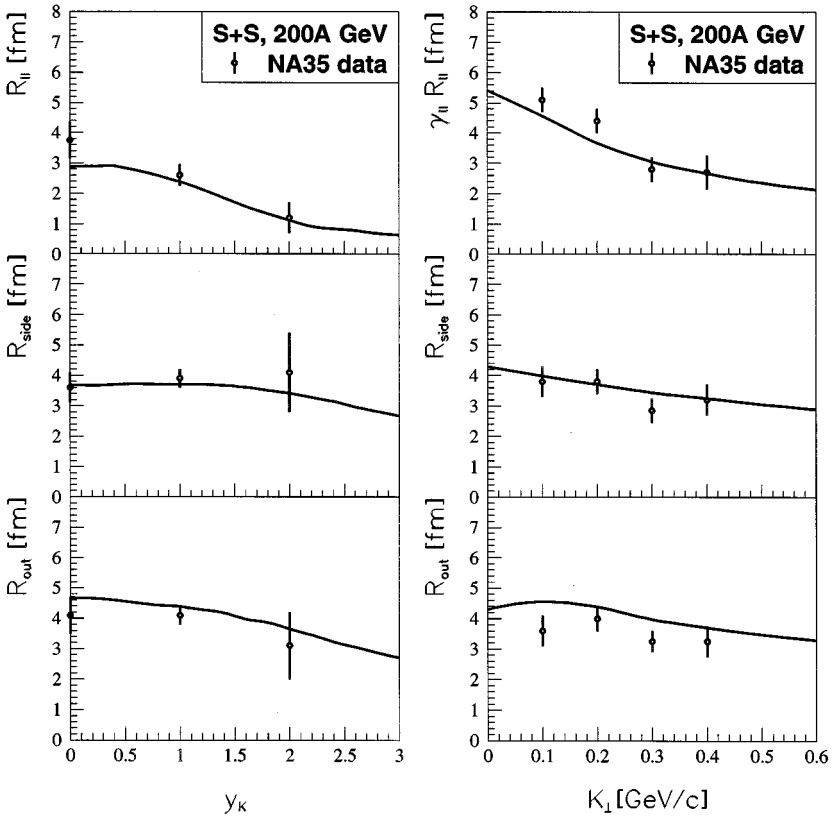

FIG. 9. Effective radii extracted from Bose-Einstein correlation functions as a function of the rapidity y_K of the pair and the transverse average momentum $K_\perp$ of the pair for all pions compared to NA35 data [11,12].

BEC's take their maximum values at low momenta. Therefore, we have strong evidence that one cannot extract the maximal effective radii of the hadron sources from the Bose-Einstein correlation data obtained at the CERN/SPS since the acceptances of the experiments do not obtain data at $y_K=0.0$ and $K_\perp=0.0$. It is important to note that in the case of the pion interferometry, the presence of a resonance halo increases the size of the fireball in the central region by factors ~ 2.1 (~ 2.0) in longitudinal and ~ 1.4 (~ 1.3) in transverse direction for Pb+Pb (S+S). Values for the maximal possible resonance halo size are given in Table I.

In Fig. 11 we show a two-particle Bose-Einstein correlation function $\widetilde{C}_2(Q_{\rm inv})$ as a function of the invariant variable $Q_{\rm inv}$. This BEC function is defined as follows (cf. also Refs. [16,17,29]). Let $\rho_2(\vec{k}_1,\vec{k}_2)$ be the inclusive two-particle spectrum for two identical pions with momenta $\vec{k}_1$ and $\vec{k}_2$ and $\rho_1(\vec{k})$ the inclusive single-particle spectrum for a pion with momentum $\vec{k}$, respectively:

$$\rho_1(\vec{k})=\frac{1}{\sigma}\frac{d\sigma}{d\omega},\quad \rho_2(\vec{k}_1,\vec{k}_2)=\frac{1}{\sigma}\frac{d^2\sigma}{d\omega_1 d\omega_2},$$
$$d\omega=\frac{d^3k}{(2\pi)^3\times 2E}. \tag{7}$$

The two-particle BEC for a single pair of two pions with momenta $\vec{k}_1$ and $\vec{k}_2$ takes the form

$$C_2(\vec{k}_1,\vec{k}_2)=\frac{\rho_2(\vec{k}_1,\vec{k}_2)}{\rho_1(\vec{k}_1)\cdot\rho_1(\vec{k}_2)}=1+\frac{\overline{c(\vec{k}_1,\vec{k}_2)}}{\rho_1(\vec{k}_1)\cdot\rho_1(\vec{k}_2)}. \tag{8}$$

The separate contributions $\overline{c(\vec{k}_1,\vec{k}_2)}$, $\rho_1(\vec{k}_1)$, and $\rho_1(\vec{k}_2)$ have to be calculated for each pair of pion momenta including also the interference contributions from the pions which originate from the decay of resonances (cf. Refs. [9,10,17]).

The two-particle Bose-Einstein correlation function $\widetilde{C}_2(Q_{\rm inv})$ as a function of the invariant variable $Q_{\rm inv}$ is given by

$$\widetilde{C}_2(Q_{\rm inv})=1+\frac{I_2(Q_{\rm inv})}{I_{11}(Q_{\rm inv})}. \tag{9}$$

With $q^\mu=k_1^\mu-k_2^\mu$ we have

$$I_{11}(Q_{\rm inv})=\int d\omega_1\int d\omega_2\,\delta[Q_{\rm inv}-\sqrt{-q^\mu q_\mu}]\rho_1(\vec{k}_1)\rho_1(\vec{k}_2),$$
$$I_2(Q_{\rm inv})=\int d\omega_1\int d\omega_2\,\delta[Q_{\rm inv}-\sqrt{-q^\mu q_\mu}]\overline{c(\vec{k}_1,\vec{k}_2)}, \tag{10}$$

and k^μ represents the four-momentum of a pion. The integrations have to take into account the particular detector acceptance for the experiment under consideration. Here we considered the phase space $1.1\leqslant y\leqslant 2.1$ and 50 MeV $\leqslant k_\perp\leqslant 600$ MeV, which covers the detector acceptance of the NA49 experiment.

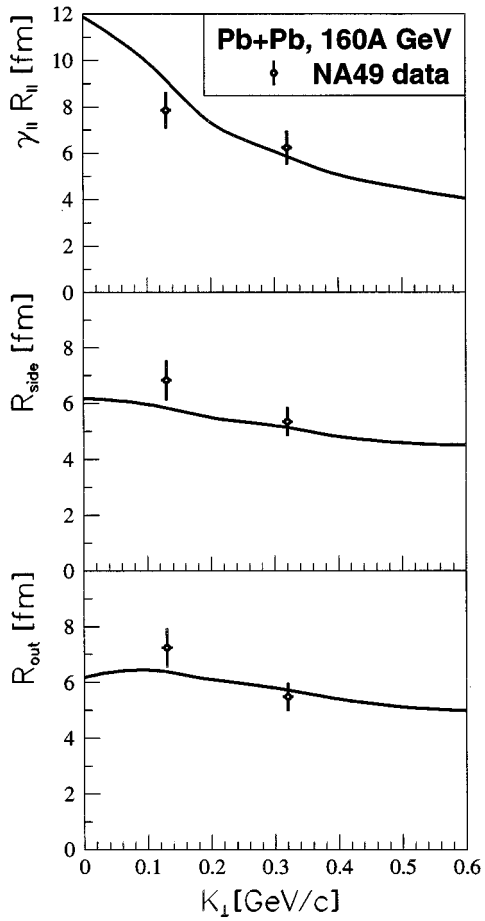

FIG. 10. Effective radii extracted from Bose-Einstein correlation functions as a function of the transverse average momentum $K_\perp$ of the pair for all pions compared to preliminary NA49 data [12].

In the previous section we mentioned that in the case of pion interferometry we have to deal with a large fraction, 40%–50%, of the pions originating from resonances. This statement refers to an average over all particle momenta. In case of the NA49 detector acceptance the main contributions to the two-pion BEC come from thermal π^- (72.8%) and π^- contributions from ρ (15.6%), ω (8.7%), and η decays (2.9%). The effects of resonance decays on the two-particle Bose-Einstein correlation function $\widetilde{C}_2(Q_{\rm inv})$ are also shown in Fig. 11, where we successively have added contributions from the specific resonance decay channels to the thermal (direct) pion contributions. The more resonances we take into account, the narrower the correlation function becomes because the addition of a resonance halo increases the effective source size (cf. Refs. [9,10,15]). As discussed in our earlier papers, the resonance contributions from the η resonance yield an apparent intercept reduction. The intercept $I_0=\widetilde{C}_2(Q_{\rm inv}=0)$ of the BEC takes the value $I_0\approx 1+0.97^2\approx 1.94$ (cf. also Ref. [10]). Here we do not compare our numerical result to the preliminary data of the NA49 Collaboration [12], because the current experimental correlation function represents a data sample of only 529 events. Furthermore, we believe that there may be problems in the preliminary data with the experimental two-track resolution and/or Coulomb overcorrections that are apparent at

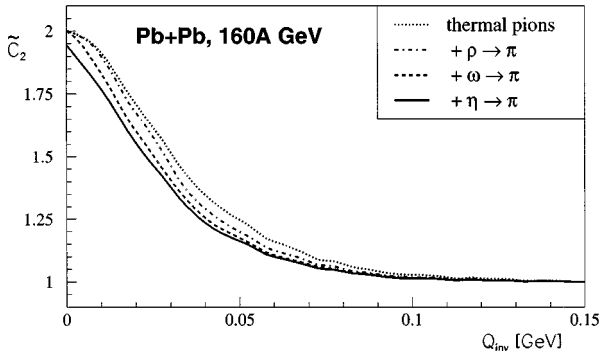

FIG. 11. Two-particle Bose-Einstein correlation functions $\widetilde{C}_2(Q_{\rm inv})$ of negatively charged pions. The contributions from resonance decays are successively added to the correlation function of thermal π^- (dotted lines). The resultant correlation function of all π^- is given by the solid line. The integrations have been performed with respect to the detector acceptance of the NA49 experiment (see text).

very small values of $Q_{\rm inv}$. Nevertheless, the present particular calculation demonstrates the complexity of BEC functions as they emerge from measurements.

In general, we expect the observed two-particle BEC to be strongly dependent on detector acceptances as well on the particular contributions from the decay of resonances. Bose-Einstein correlations are a very complicated observable defined through quantum statistics. These functions depend per definition on the choice of momenta under consideration. In general, different detector acceptances in different experimental setups should lead for the same heavy-ion collision at a fixed reaction energy to different results. Thus, the interpretation of BEC measurements is also complicated. The interpretation of extracted inverse widths (effective radii) of experimental BEC's depends on the specific detector acceptance under consideration. Therefore, rather than interpret experimental fitted quantities such as effective source radii, we propose the reader should pay attention to the model which analyzes the data. From the hydrodynamical treatment we learn that the hadron source (the real fireball) is represented through a very complex freeze-out hypersurface (cf. Figs. 4 and 5). The longitudinal and transverse extensions of the fireball change dynamically as a function of time, rather than show up in static effective radii. A future study [30] of the BEC's for both pions and kaons for two different detector acceptances (which could be done by considering simultaneously the experimental results of the NA49 and the NA44 Collaborations) is in preparation.

V. SUMMARY

We have shown that data from two different heavy-ion experiments for single and double inclusive cross sections of mesons and baryons can be reproduced with a self-consistent three-dimensional relativistic hydrodynamic description assuming an equation of state with a phase transition to a QGP. Our data analysis indicates a stronger stopping and an enhanced transverse flow in the case of Pb+Pb collisions compared to S+S collisions at CERN/SPS energies. In particular, the preliminary Pb+Pb data can be explained by simple

scaling assumptions in the initial conditions coming from S+S, although the final distributions do not show these scaling features [e.g., compare the final rapidity spectra of protons (cf. Fig. 7)].

Bose-Einstein correlation functions for pions have also been calculated. The NA35 and NA49 data on interferometry are surprisingly well described. Because the largest contributions to BEC from resonance decays are at small particle momenta, the current BEC experiments at CERN do not measure the maximal possible interferometry radii for identical pions. We also exhibit the freeze-out hypersurfaces; these surfaces rather than the effective radii extracted from experimentally measured BEC functions represent the true space-time geometries of the sources. This caveat should always be kept in mind when trying to interpret the BEC data.

The results of this work constitute further evidence that heavy-ion collisions in the SPS region show fluid dynamical behavior and can be described by assuming an equation of state with a phase transition from QGP to hadronic matter. This result has to be regarded in line with previous hydrodynamical studies of the Marburg group [1,2,7,9,13,14] and from other groups [31]. Of course, the EOS we have chosen might not be the only one which is able to describe the current SPS heavy-ion data. Further analysis which allows for different equations of state is in preparation [32].

ACKNOWLEDGMENTS

We would like to thank B.V. Jacak, J.P. Sullivan, and N. Xu for many helpful discussions. This work was supported by the University of California and the Deutsche Forschungsgemeinschaft (DFG). B.R.S. acknowledges a DFG postdoctoral fellowship and R.W. is indebted to A. Capella for the hospitality extended to him at the LPTHE, Univ. Paris-Sud.

[1] B.R. Schlei, U. Ornik, M. Plümer, D. Strottman, and R.M. Weiner, Phys. Lett. B **376**, 212 (1996).
[2] U. Ornik, F. Pottag, and R.M. Weiner, Phys. Rev. Lett. **63**, 2641 (1989).
[3] For a review see, for instance, R.B. Clare and D.D. Strottman, Phys. Rep. **141**, 177 (1986), and references therein; H. Stöcker and W. Greiner, *ibid.* **137**, 277 (1986), and references therein.
[4] For (3+1)-dimensional relativistic one-fluid-dynamics see, for instance, [2]; T.L. McAbee, J.R. Wilson, J.A. Zingman, and C.T. Alonso, Mod. Phys. Lett. A **4**, 983 (1989); N.S. Amelin *et al.*, Phys. Rev. Lett. **67**, 1523 (1991); B. Waldhauser *et al.*, Z. Phys. C **54**, 459 (1992); D. Strottman, Nucl. Phys. **A566**, 245c (1994); L.V. Bravina, N.S. Amelin, L.P. Csernai, P. Levai, and D. Strottman, *ibid.* **A566**, 461c (1994); R. Venugopalan, M. Prakash, M. Kataja, and P.V. Ruuskanen, *ibid.* **A566**, 473c (1994) .
[5] For relativistic multi-fluid-dynamics see, for instance, A.A. Amsden, A.S. Goldhaber, F.H. Harlow, and J.R. Nix, Phys. Rev. C **17**, 2080 (1978); L.P. Csernai *et al.*, *ibid.* **26**, 149 (1982); I.N. Mishustin, V.N. Russkikh, L.M. Satarov, in International Review of Modern Physics, **5** (edited by L.P. Csernai, D.D. Strottman (World Scientific, Singapore, 1991), p. 180; U. Katscher *et al.*, Z. Phys. A **346**, 209 (1993).
[6] L.D. Landau and E.M. Lifschitz, *Fluid Mechanics* (Pergamon, New York, 1959).
[7] J. Bolz, U. Ornik, and R.M. Weiner, Phys. Rev. C **46**, 2047 (1992).
[8] S. Wenig, Ph.D. thesis, GSI-Report No. 90-23 1990.
[9] J. Bolz, U. Ornik, M. Plümer, B.R. Schlei, and R.M. Weiner, Phys. Lett. B **300**, 404 (1993).
[10] J. Bolz, U. Ornik, M. Plümer, B.R. Schlei, and R.M. Weiner, Phys. Rev. D **47**, 3860 (1993).
[11] Th. Alber *et al.*, Phys. Rev. Lett. **74**, 1303 (1995); Th. Alber *et al.*, Z. Phys. C **66** 77 (1995).
[12] NA35 and NA49 Collaborations, T. Alber, Nucl. Phys. **A590**, 453c (1995); T. Alber *et al.*, Phys. Rev. Lett. **75**, 3814 (1995).
[13] N. Arbex, U. Ornik, M. Plümer, A. Timmermann, and R.M. Weiner, Phys. Lett. B **345**, 307 (1995).
[14] U. Ornik and R.M. Weiner, Phys. Lett. B **263**, 503 (1991).
[15] T. Csörgő, B. Lörstad, and J. Zimányi, Z. Phys. C (to be published).
[16] I.V. Andreev, M. Plümer, B.R. Schlei, and R.M. Weiner, Phys. Lett. B **316**, 583 (1993).
[17] I.V. Andreev, M. Plümer, B.R. Schlei, R.M. Weiner, Phys. Rev. D **49**, 1217 (1994).
[18] B.R. Schlei, U. Ornik, M. Plümer, and R.M. Weiner, Phys. Lett. B **293**, 275 (1992).
[19] L.D. Landau, Ivz. Akad. Nauk SSSR **17**, 51 (1953).
[20] J.D. Bjorken, Phys. Rev. D **27**, 140 (1983).
[21] K. Redlich H. Satz, Phys. Rev. D **33** 3747 (1986).
[22] U. Ornik, Ph.D. thesis, Universität Marburg, 1990.
[23] B. R. Schlei, Ph.D. thesis, Universität Marburg, 1994.
[24] F. Cooper, G. Frye, and E. Schonberg, Phys. Rev. D **11**, 192 (1975).
[25] S. Margetis and the NA49 Collaboration, Nucl. Phys. **A590**, 355c (1995).
[26] NA49 Collaboration, ''First Results from Experiment NA49 at the CERN-SPS Lead Beam,'' GSI-Nachrichten Report No. GSI 06-95 1995, pp. 8–16.
[27] NA44 Collaboration, B.V. Jacak and N. Xu (private communication).
[28] S. Chapman, P. Scotto and U. Heinz, Phys. Rev. Lett. **74**, 4400 (1995).
[29] P. Grassberger, Nucl. Phys. **B120**, 231 (1997).
[30] B.R. Schlei, D. Strottman, and R.M. Weiner (unpublished).
[31] N.S. Amelin *et al.*, Phys. Lett. B **261**, 352 (1991); N.S. Amelin *et al.*, Phys. Rev. Lett. **67**, 1523 (1991); T. Ishii and S. Muroya, Phys. Rev. D **46**, 5156 (1992); E. Shuryak and L. Xiong, Phys. Lett. B **333**, 316 (1994); D.K. Srivastava and B. Sinha, Phys. Rev. Lett. **73**, 2421 (1994); A. Dumitru *et al.*, Phys. Rev. C **51**, 2166 (1995).
[32] B.R. Schlei and D. Strottman (unpublished).